Met. Mater. Int., Vol. 23, No. 3 (2017), pp. 473~480
doi: 10.1007/s12540-017-6686-9

Depth Sensing Indentation Analyses of Hypereutectic Al-10Ni – XSc (X = 0, 1, 2) Alloys

M. Fatih Kilicaslan[1,*] and Ercan Karakose[2]

[1]Department of Materials Science and Nanotechnology Engineering, Faculty of Engineering and Architecture, Kastamonu University, Kastamonu 37200, Turkey
[2]Department of Physics, Faculty of Sciences, Çankırı Karatekin University, Cankiri 18200, Turkey

(received date: 28 September 2016 / accepted date: 19 November 2016)

Depth sensing indentation analyses of hypereutectic Al-10Ni alloys with different amounts of Sc content were performed to determine the values of elastic modulus, dynamic microhardness, creep rate and elastic recovery rate. Microstructural characterizations were performed by using scanning electron microscopy (SEM), SEM mapping and an X-ray diffractometer. The results revealed that the addition of Sc refined the intermetallic phases of Al and Ni, and led to the formation of two additional intermetallic phases as well, namely Al_3Sc and metastable Al_9Ni_2. The Al-Ni alloys investigated in this work exhibited elastoplastic behavior at room temperature and the addition of Sc influences their elastic-plastic responses to the indentation process. In addition, dynamic microhardness of them exhibited a load-dependent character called the indentation size effect. The addition of Sc considerably improved the values of dynamic microharddness, elastic modulus and elastic recovery rate. It also resulted in a lower creep displacement rate.

Keywords: microstructure, indentation, creep, mechanical properties, dynamic microhardness

1. INTRODUCTİON

Constructional materials with preferential mechanical properties like high corrosion resistance, low density, and a relatively high temperature strength are very important for the automotive and aviation industries. These needs, connected with economic aspects, have led to the development and utilizations of new technologies for the manufacture of various aluminum alloys [1,2]. Nowadays, the legislation concerning exhaust emissions recommends the development of automotive engines with high efficiency, which has put pressure on R&D researchers to improve the best performance pistons and cylinder blocks [3]. Among aluminum alloys, hypereutectic Al–Ni alloys have the superior corrosion and abrasion resistance, high elevated temperature strength and a low coefficient of thermal expansion which makes them a good candidate for automotive and aviation applications [4-7]. It has been reported that Al-Ni alloys contain intermetallics Al_3Ni, Al_3Ni_2 and Al_9Ni_2 phases, which are classified as geometrically close packed structures illustrating morphological stability up to their melting point due to weak diffusion of the atomic structures [8]. For this reason, Al-Ni intermetallic alloys have good high-temperature characteristics. However, these alloys also have considerable disadvantages, like low toughness and ductility at room temperature. Therefore, in recent years many studies have been conducted on eliminating the detrimental effects of acicular and faceted Al and Ni intermetallics, and these studies have reported that the addition of a small amount of Cu, Mg, Si and Zr as ternary elements enhances the mechanical properties of Al–Ni alloys at room temperature [9-11]. Sc is one of the most important grain refiners of the cast particle in aluminum castings [12] because it limits grain boundary growth in the heat region of welded Al components. Also, precipitated Al_3Sc intermetallics which have a smaller lattice parameter compared to other intermetallics phases increased frequency of heterogeneous nucleation for both intermetallics and aluminum phases, resulting in a refined and modified microstructure [13]. Venkateswarlu *et al.* [14] found that Sc addition to Al exhibited excellent results in terms of grain refinement compared to the addition of AlTiB master alloy. Additions of Zr and Sc in Al alloys may also decrease the particle sizes of Al-Mg-Si-Mn samples [15,16]. However, the effects of Sc on the morphological characteristics of Al-Ni alloys have rarely been investigated. To the best of our knowledge, there is no study in the literature in which 1, 2% Sc has been added to Al–10Ni alloy.

On the other hand, the modulus of elasticity, which is a mathematical description of the responses of a material or machine part to elastic deformation when a force is applied

*Corresponding author: fkilicarslan@kastamonu.edu.tr

to it, is one of the most important parameter in terms of numerous technological applications. The modulus of elasticity can be calculated by different methods. One of the most practical methods to determine elastic modulus is depth sensing indentation (DSI). In addition, by using the DSI technique, it is possible to determine other important parameters such as dynamic microhardness, creep displacement rate, elastic recovery. Furthermore, in the open literature, according to the best of our knowledge, the dynamic mechanical properties of hypereutectic Al-10Ni- XSc (X = 0, 1, 2) alloy have been rarely reported. Therefore, the purpose of this study was to examine the effects of the addition of Sc on the morphological and mechanical properties of Al-10Ni alloys with different amount of Sc.

2. THEORETICAL BACKGROUND

In Fig. 1, it is given a schematic illustration of indentation load (P) versus penetration depth (h) data obtained during one full cycle of the loading and unloading process. In this process, some of the important parameters are peak load (P_{max}), the maximum penetration depth (h_{max}), the final or residual depth after unloading (h_f), contact depth (h_c). Two important mechanical properties, the hardness (H) and elastic modulus (E), which are two important mechanical properties of materials can be determine from the loading and unloading data using the following equations:

$$H = \frac{P_{max}}{A};\ A = 26.43h_c^2 \tag{1}$$

where A is the contact area at the given load and

$$E = \frac{s}{2}\sqrt{\frac{\pi}{A}} \tag{2}$$

where E is the elastic modulus.

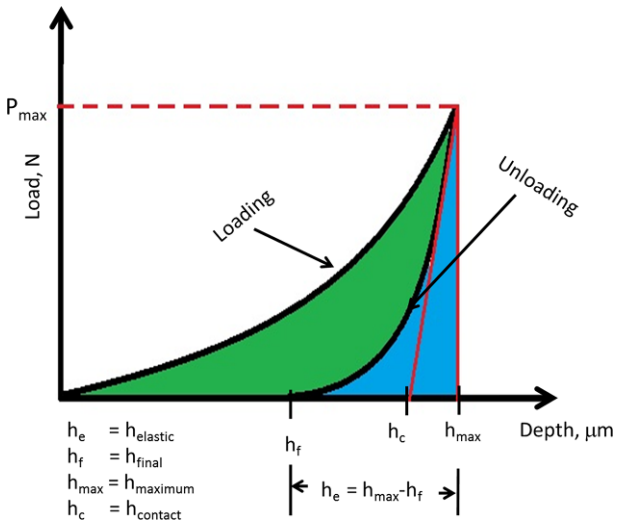

Fig. 1. Schematic illustration of indentation load (P) vs penetration depth data obtained during one full cycle of loading and unloading process.

Table 1. Chemical compositions of the as-cast Al-Ni alloys

Sample	Ni (wt%)	Sc (wt%)	Al (wt%)
AN0	10.0	0.0	bal.
AN1	10.0	1.0	bal.
AN2	10.0	2.0	bal.

3. MATERIAL AND METHODS

The Al-10Ni alloys with different amount of Sc used for this investigation were induction melted under an argon atmosphere from starting materials of elementel Al (99.9% purity), Ni (99.99% purity), and Sc (99.99% purity). For the peresent work, all percentages are weight percents unless otherwise staded. Samples with no Sc, and additions with 1 and wt% Sc were denoted as AN0, AN1 and AN2 respectively. All of the samples produced are shown in Table 1. The microstructure and phase identification of the samples were investigated by using FEI Quanta FEG 250 scanning electron microscopy with energy dispersive spectrometry, a Bruker D8 Advance X-ray diffractometer with high energy monochromatic CuKα radiation (0.15418 nm) in the 2θ range of 20-80° at a scan rate of 0.05°/s. Indentation experiments were performed using a depth-sensing indentation instrument with a Vickers tip (Bruker UMT-2 SYS). All tests were performed under the same operating conditions. For all samples, the maximum load was 5N and the holding time for creep experiments was 10s at each peak load.

4. RESULTS AND DISCUSSION

While the SEM micrographs given in Fig. 2 illustrate the microstructural evolution of conventional cast Al-Ni alloys with the addition of Sc, Fig. 3 illustrates the XRD patterns from these samples. While Fig. 2(a) shows the SEM micrograph of Sc free alloy Al-10Ni (AN0), Figure 2(b and c) shows the SEM micrographs of alloys containing 1 (AN1) and 2 (AN2) wt% Sc, respectively. According to the SEM micrographs and XRD analyses, the microstructure of the as-cast Al-10Ni alloys consisted of α-Al matrix and intermetallic compounds with elliptical, particle like and long rod like morphologies.

It is clearly seen from Fig. 2(a) that the microstructure of the Sc-free alloy was much coarser compared to other samples (Fig. 2(b and c)) and had a regular isotropic orientation. In the sample AN0, the lengths of the particle - like, elliptical and rod - like intermetallics changed from 10 μm to 18 μm, from 18 μm to 28 μm, and from 30 μm to 151 μm, respectively, whereas, their widths were around 18 μm (Fig. 2(a)). In Fig. 2(b) it is clearly seen that with the addition of 1 wt% Sc, the width and length of the intermetallics decreased drastically and also orientation of them changed and became more irregular. Lengths of particle - like, elliptical and rod like intermetallics changed from 4 μm to 8 μm, from 8 μm to 13 μm, and from 17 μm to 56 μm, respectively. The average width of the intermetallics

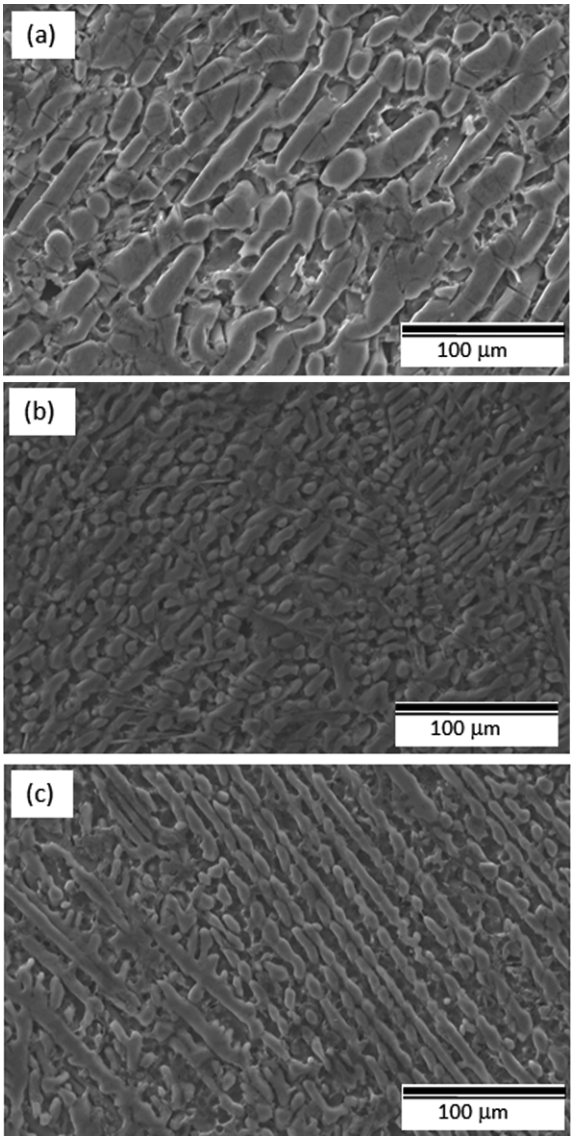

Fig. 2. SEM micrographs of Al-10Ni alloys with different amounts of Sc; (a) Sc-free (AN0), (b) alloys with 1 and 2 wt% Sc content (b and c), respectively.

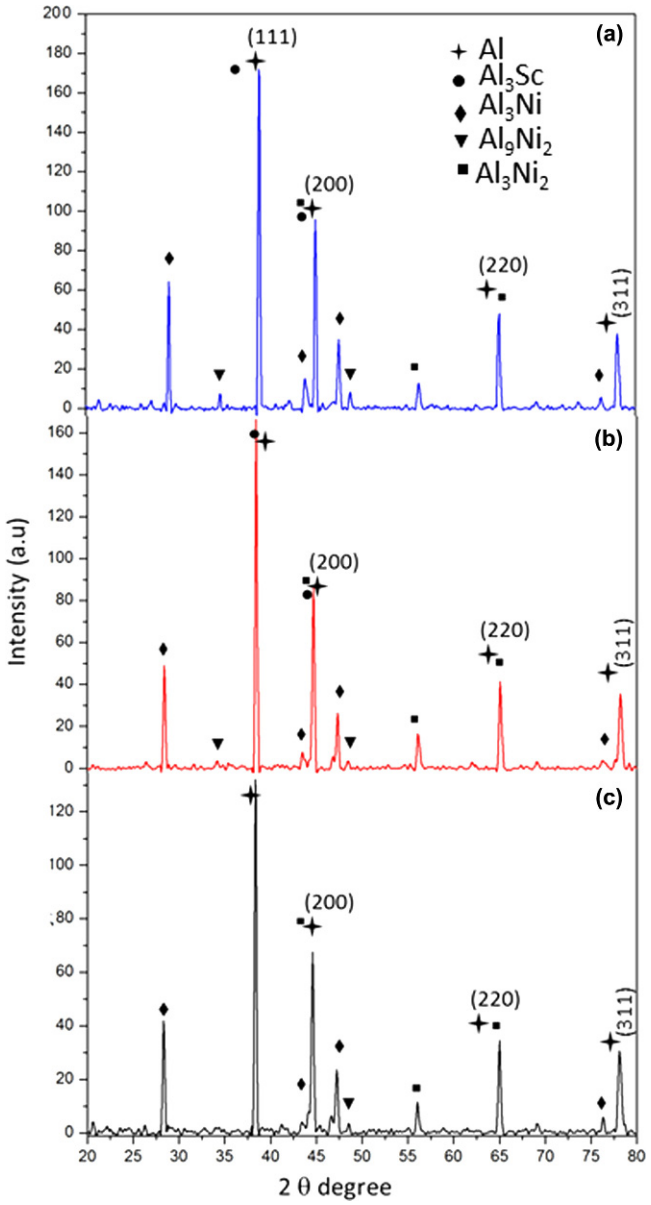

Fig. 3. X-ray diffraction patterns of samples (a) AN2, (b) AN1, and (c) AN0.

was around 7 µm (Fig. 2(b)). In the microstructure of sample AN2, with the addition of 2 wt% Sc, the width of the intermetallics did not change considerably; it was around 8 µm on average. However, the length of the particle, elliptical and rod like intermetallics remarkably changed from, 7 µm to 12 µm, from 13 µm to 23 µm, and from 40 µm to 150 µm, respectively, (Fig. 1(c)). In the microstructure of sample AN2 (Fig. 2 (c)), the orientations of all intermetallics again became isotropic and were nearly the same as the Sc-free alloy AN1 (Fig. 2(a)), and we had an impression from Fig. 2(c) that long rod-like intermetallics were formed by the combination of individual elliptical or particle- like intermetallics during solidification.

From the XRD patterns, it can be concluded that the microstructure of the Sc free alloy (AN0) contained only two kinds of intermetallic compounds, namely Al_3Ni and Al_3Ni_2; however, those alloys containing Sc, namely AN1 and AN2, include the intermetallic phases of Al_3Ni, Al_3Ni_2 Al_9Ni_2 and Al_3Sc, which is agreement with refs [17-19]. This means that the addition of Sc led to formation of two additional intermetallic pleases, namely Al_9Ni_2 and Al_3Sc. According to the Al-Sc phase diagram for an aluminum alloy having 1 and 2 wt% Sc, the formation of the Al_3Sc intermetallic phase can be anticipated [20]. However, the formation of the Al_9Ni_2 phase under equilibrium condition is not normal in the Al-Ni system. In binary Al-Ni system, it is reported that the Al_9Ni_2 phase occurs as a part of the aluminum-rich side within the binary Al-Ni phase diagram under non-equilibrium rapid solidification conditions [18]. It is well known from literature that under rapid

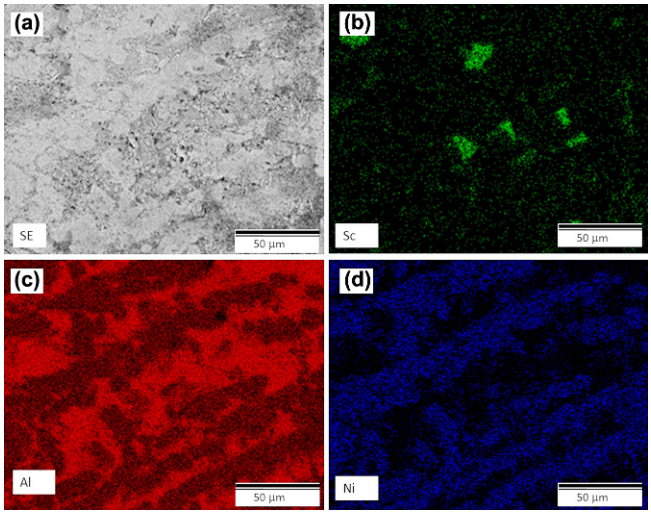

Fig. 4. SEM mapping analyses from sample AN1; (a) SE micrograph, distributions of Sc (b), Al (c), and Ni (c), respectively.

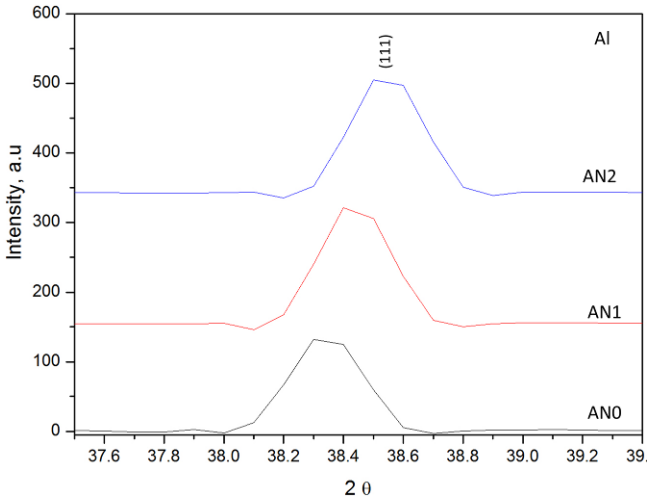

Fig. 5. X-ray diffraction patterns of samples AN0, AN1 and AN2 illustrating the peaks with the highest intensity of Al (111).

solidification conditions, metastable intermetallic phases can be formed because of an increased undercooling level caused by a very high cooling rate [21,22]. It is also reported in the literature that when Sc is added to Al alloys, an increased Sc concentration in the liquid phase leads to greater constitutional undercooling [23,24]. Hence, in our situation, it could be asserted that the metastable Al_9Ni_2 phase is formed due to the higher constitutional undercooling caused by Sc addition.

Figure 4 shows the maps of Ni and Sc from the AN1 alloy. As shown in Fig. 4, the rod- like phases embedded in the Al matrix were Ni-rich. However, some facet structured particles containing Sc were distributed in the microstructure, and it can also be concluded from Fig. 4 that in the same region with Ni rich phases, there were also traces of Sc as well. This mean that Ni containing intermetallic phases can also include Sc in AN1 and AN2 alloys, which is in agreement with ref. [18].

The calculated lattice parameters and FWHMs (full width at half maximum) obtained from the Al (111) peaks of AN0, AN1 and AN2 alloys are given in Table 3, while Fig. 5 shows the peaks with the highest intensity of Al (111). It is clearly seen from Table 3 and Fig. 5 that compared to the Sc-free alloys (AN0), the Al (111) peaks shift to the right in the AN1 and AN2 samples with the addition of Sc, and the lattice parameters also get smaller with the addition of Sc. Actually, the atomic radius of Sc (162 pm) is bigger compared to Al (143 pm), however the atomic radius of Ni (124 pm) is smaller than that of Al [25]. On the other hand, it is known from the literature that an increased Sc concentration in the liquid phase leads to greater constitutional undercooling, in Al alloys. Also, an increase in undercooling level results in an increase in solute solubility limits [23,24]. Therefore, we think that the increased constitutional undercooling caused by the addition of Sc extended the solute solubility limits and brought about dissolution of a higher amount of Ni in the Al matrix, resulting in a decrease

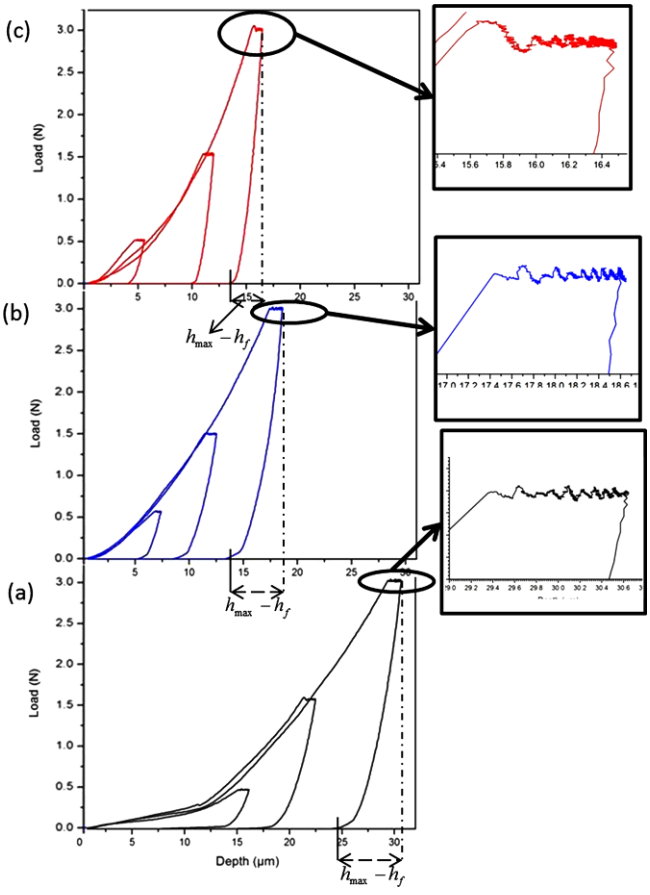

Fig. 6. Loading - unloading curves of as-cast Al-10Ni alloys with different amount Sc addition obtained from dynamic micro indentation tests; (a) Sc-free (AN0), (b) alloys with 1 (AN1) and 2 (AN2) wt% Sc content (b and c), respectively.

in lattice parameter. FWHMs of Al (111) were found in the following order (Table 3): AN0 <AN1<AN2. In the literature, broadening of Al (111) peak is attributed to the reduc-

Table 2. Mechanical properties calculated under different peak loads of Al-Ni-Sc alloys

Load (N)	Al-Ni			Al-Ni-1Sc			Al-Ni-2Sc		
	Microhardness (GPa)	Elastic Modulus (GPa)	Creep (μm)	Microhardness (GPa)	Elastic Modulus (GPa)	Creep (μm)	Microhardness (GPa)	Elastic Modulus (GPa)	Creep (μm)
0.5	0.191	9.293	1.00	0.510	24.5424	0.92	0.480	17.620	0.70
1.5	0.142	6.720	1.20	0.402	19.8072	0.99	0.456	16.149	1.10
3.0	0.137	6.280	1.35	0.364	18.396	1.01	0.419	15.77	1.19

Table 3. Values of h_f/h_{max} and h_{max}-h_f calculated for 3 N maximum loading

	h_f/h_{max}	h_{max}-h_f (μm)	Lattice parameter (a)	FWHM
Al-Ni	0.822	5.4	0.40628	0.272
Al-Ni-1Sc	0.737	4.9	0.40540	0.280
Al-Ni-2Sc	0.818	3.0	0.40460	0.289

tion in the crystal size of Al phase.

The representative loading-unloading curves recorded from the dynamic microindentation tests of samples AN0, AN1 and AN2 are given in Fig. 6. It can be clearly seen from the Fig. 6 that our samples exhibited elastoplastic behavior at room temperature and the addition of Sc affected their elastic-plastic responses to the indentation process [21]. Figure 6 also shows that loading curves under different maximum loads can be fitted by one curve due to their overlapping characters. The unloading part of the loading-unloading curves also exhibits similar behavior when they are shifted according to their final penetration depths. In the literature, such overlapping characters of loading-unloading curves are interpreted as showing that the sample has similar elastic and plastic deformation mechanism for the given experimental load range [21,22]. It could also be concluded from Fig. 7 and Table 2 that the dynamic microhardness values decreased with increasing peak load. This phenomenon is known as the indentation size effect (ISE) [26]. The slope of the loading curve for the sample AN0 (Fig. 6(a)) was lower compared to other two samples. In samples AN1 and AN2, with Sc addition (Fig. 6(b and c)), the slope

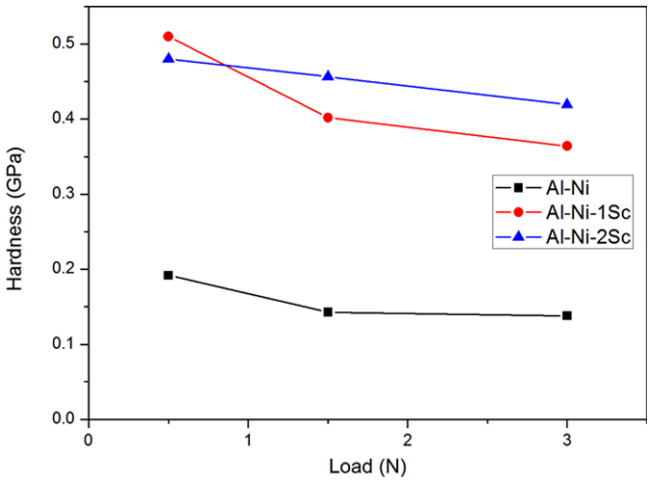

Fig. 7. Changes in the dynamic microhardness values of as-cast Al-Ni alloys with different amount of Sc addition.

of the loading curve increased with increasing Sc addition, referring to the enhanced strain hardening ability in a small volume of as-cast Al-10Ni alloys [23]. Shifting of the unloading portions to a higher indentation depth implies that higher plastic deformation occurs during indentation. One description of hardness is the resistance of materials to plastic deformation [24]. Hence, from the loading-unloading curves, ther microhardness of the samples can simply be arranged in order as AN0< AN1<AN2. On the other hand, Table 2 shows the dynamic microhardness values calculated using Eq. (1). The changes in the dynamic microhardness values of the sample with the addition of Sc are consistent with the above results and are seen in Fig. 7. It is well known from literature that modification and refining of the secondary phases in microstructure reduce the probability of crack formation and enhance the mechanical properties [27,28]. Hence, particle size strengthening caused by the addition of Sc, which led to refining of coarse intermetallics (Fig. 2), could be one possible reason for the increment in the dynamic microhardness values. On the other hand, the addition of Sc led to the highest increment of strengthening per atom percent in aluminum because Sc addition induced the solid solution and precipitation hardening of Al_3Sc particles [29]. Our samples contain 1 and 2 wt% Sc, whereas, the maximum solid solubility of Sc in Al was 0.35 wt%. Therefore, other possible reasons for the increment in the dynamic microhardness values can be solid solution and precipitation hardening.

While Fig. 8 shows changes in the elastic modulus (E) of as- cast Al-10Ni alloys with the addition of Sc, Table 2 shows the elastic modulus values which indicated that the addition of Sc brought about a significant increment in the elastic modulus. In the AN1 sample, the addition of 1 percent Sc led to highest elastic modulus values which were approximately three times higher than those of the Sc-free alloy (AN0). However, when the amount of Sc addition increased from 1 to 2 percent, the elastic modulus values decreased considerably, however, they were still double those of the Sc-free alloy (AN0). One of the intrinsic properties of materials is elastic modulus, which

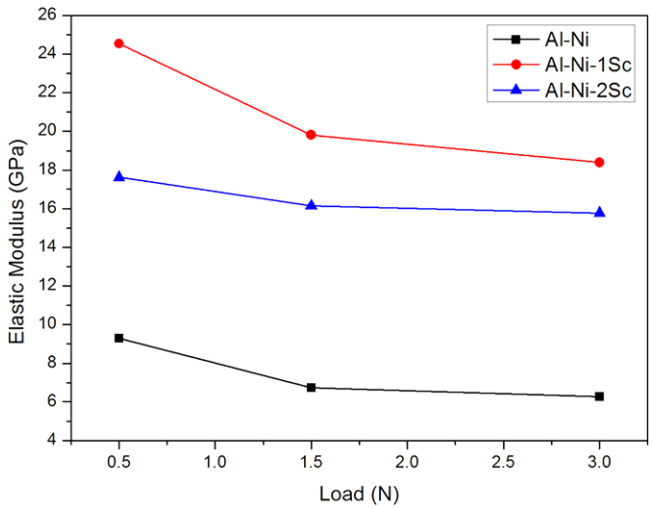

Fig. 8. Changes in the elastic modulus (*E*) values of as- cast Al-Ni alloys with different amount of Sc addition.

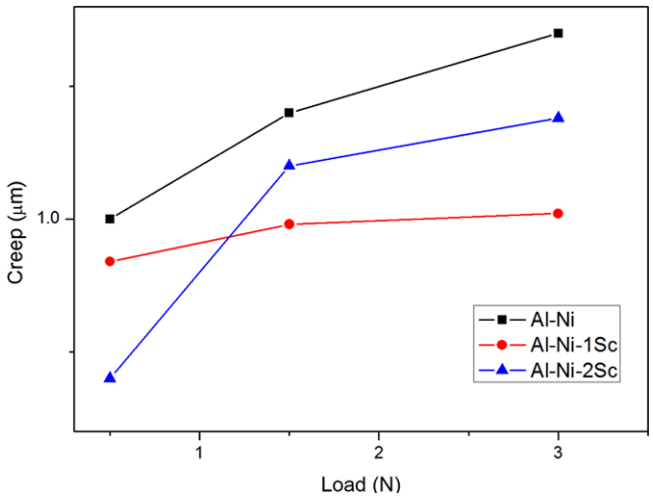

Fig. 9. Changes in the creep rate of as- cast Al-Ni alloys with different amount of Sc addition.

is related to the bonding forces among atoms. The bonding force between atoms is determined not only by the crystal structure but also by interatomic spacing, and it can also be affected by alloying additions [30]. Royset and Ryum [31] reported that since Sc is located close to Ti, and Zr in the periodic table, these three elements have a few similarities in terms of interactions with Al. Wang *et al.* [32] reported that both Ti and Zr brought about an increment in the value of the bulk modulus of Al alloys. Therefore, we believe that the addition of Sc led to an increase in the elastic modulus of Al-10Ni alloys with a mechanism similar to that in Ti and Zr. On the other hand, Alhayek and Gaith [33] stated in their work that bulk modulus was inversely proportional to the lattice constants for ZnX (X = S, Se, Te) alloys, which is in agreement with the results of the present study since with addition of Sc lattice parameter decreased (Table 3) and the elastic modulus increased. However, when Sc addition was increased 1 to 2 wt%, a decrease was observed in the elastic modulus values and the reason for this was unclear.

One of the important experimentally measurable parameter is the ratio between final penetration depth (h_f) and penetration depth at peak load (h_{max}). Note that ratio of h_f/h_{max} can be easily obtained from the unloading curves of each cycle and used as a criterion to determine deformation mode. Accordingly, h_f/h_{max} ratio is a practical indicator of pile-up or sink-in deformation modes around the indenter. When the h_f/h_{max} value is higher than the critical value of 0.7, pile-up is the dominant deformation mode. On the other hand, sink-in behavior is significant when the h_f/h_{ma} parameters have a value less than 0.7 [26]. Table 3 shows the h_f/h_{max} values of the samples in the present study. As it can be seen, for all of the samples the h_f/h_{max} values were higher than the critical value of 0.7, which indicates that the deformation mode of the samples is pile-up around the indenter. It was reported that smaller peak loads led to more pronounced pile-up values. Also severe material pile-up induces over estimation of the calculated microhardness [34]. There for, in our case, the possibility of obtaining inaccurate data and calculating overestimated dynamic microhardness was the highest during applying 0,5N load which was the smallest peak load. It can already be seen from Fig. 6 that in the loading parts of curves for 0,5N peak loads, there were considerable distortions (especially in the alloys AN0 and AN2 (Fig. 6(a and c)) which were possibly due to the pile-up effect.

Figure 9 shows changes in creep versus load for AN0, AN1 and AN2 alloys for 10s holding time, whereas the creep values are seen in Table 3. Actually, in literature, the horizontal segments in the loading-unloading curves (Fig. 6) are also a creep indicator showing the further penetration of the indenter onto the spacemen during dwell time at room temperature. Although creep normally is seen at elevated temperature, for viscous materials it can also be observed at ambient temperature [26]. From Fig. 9 and Table 3 we can conclude that for all of the samples significant creep displacement was observed, and creep displacement increased with increasing peak load. While, the highest creep displacement value belonged to the Sc-free alloy (AN0), meaning addition of Sc led to lower creep displacement, the highest variation in creep displacement with increasing peak load was observed in the sample AN2.

It is stated in literature that h_{max}, h_f, and h_{max}-h_f can be presumed as a measure of total work, plastic work and elastic work, respectively. Because unloading from h_{max} to h_f is elastic and h_{max}-h_f is related to elastic penetration depth, h_{max}-h_f can be used as a parameter which represents elastic recovery rate [23]. Elastic recovery rate values (h_{max}-h_f) are given in Table 3, and changes of them with addition of Sc are seen in Fig. 10. From Fig. 10 and Table 3 it can be observed that was gradual decrease in the elastic recovery rate with the addition of Sc.

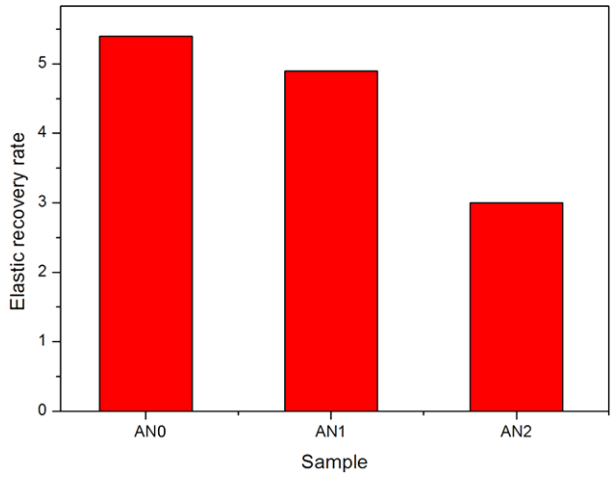

Fig. 10. Changes in the elastic recovery rate of as- cast Al-Ni alloys with different amounts of Sc addition.

5. CONCLUSION

In this study, we investigated the effects of the addition of Sc on the microstructural properties of as-cast Al-10Ni alloys and, determined the mechanical properties of all of the alloys using depth sensing indentation analyses. The results can be summarized as follows:

(1) The addition of Sc led to a considerable decrease in the size of intermetallic phase in as-cast Al-10Ni alloys.

(2) The addition of Sc led to the formation of two additional intermetallic phases, Al_3Sc and metastable Al_9Ni_2.

(3) All of the samples exhibited elastoplastic behavior at room temperature and the addition of Sc affected their elastic-plastic responses to the indentation process.

(4) It can be concluded from the overlapping characters of the loading-unloading curves that the samples had a similar elastic and plastic deformation mechanism for the given experimental load range.

(5) For all of the samples the h_f/h_{max} values were higher than the critical value of 0.7, which indicated that deformation mode of our samples was pile-up around the indenter.

(6) The dynamic microhardness values exhibited load-dependent behavior called ISE.

(7) The addition of Sc led to a considerable increment in the dynamic microhardness values due to particle size hardening and/or solid solution and precipitation hardening

(8) Compared to the Sc-free alloy (AN0), additions of 1 and 2 percent Sc led to higher elastic modulus values which were three times and double those of the AN1 and AN2 alloys, respectively.

(9) The addition of Sc led to lower creep displacement in as-cast Al-10Ni alloys.

(10) It was observed that there was a gradual decrease in the elastic recovery rate with the addition of Sc in as-cast Al-10Ni alloys.

ACKNOWLEDGEMENT

This work was supported by Kastamonu Universitesi Bilimsel Arastirma Projeleri Yonetimi Koordinatorlugu [KÜBAP-01/2013-33].

REFERENCES

1. A. A. Fahmy and A. N. Ragai, *J. Appl. Phys.* **41**, 5108 (1970).
2. M. M. Haque and M. A. Maleque, *J. Mater. Process. Tech.* **77**, 122 (1998).
3. M. Murayama, K. Hono, M. Saga, and M. Kikushi, *Mat. Sci. Eng. A* **250**, 127 (1998).
4. Y. H. Kim, A. Unoue, and T. Matsumoto, *Mater. T. JIM* **31**, 747 (1990).
5. T. Zhang, A. Unoue, and T. Matsumoto, *Mater. T. JIM* **32**, 1005 (1991).
6. Z. C. Zhong, X. Y. Jiang, and A. L. Greer, *Mat. Sci. Eng. A* **226-228**, 531 (1997).
7. F. J. Dom, *Aluminium* **70**, 575 (1994).
8. D. P. Pope and S. S. Ezz, *Int. Mater. Rev.* **29**, 136 (1984).
9. D. Srinivasan and K. Chattopadhyay, *Mat. Sci. Eng. A* **375-377**, 1228 (2004).
10. B. J. McKay, P. Cizek, P. Schumacher, and K. A. Q. O'Reilly, *Mat. Sci. Eng. A* **304-306**, 240 (2001).
11. K. L. Sahoo, M. Wollgarten, J. Haug, and J. Banhart, *Acta Mater.* **53**, 3861 (2005).
12. V. G. Davydov, T. D. Rostova, V. V. Zakharov, Y. A. Filatov, and V. I. Yelagin, *Mat. Sci. Eng. A* **280**, 30 (2000).
13. A. Zaki, *JOM* **55**, 35 (2003).
14. K. Venkateswarlu, L. C. Pathak, A. K. Ray, G. Das, P. K. Verma, M. Kumar, *et al. Mat. Sci. Eng. A* **383**, 374 (2004).
15. A. F. Norman and R. S. McEwen, *Acta Mater.* **46**, 5715 (1998).
16. J. Z. Dang, Y. F. Huang, and J. Cheng, *T. Nonferr. Metal. Soc.* **19**, 540 (2009).
17. G. Gonzalez, L. G. A. Rodriguez, S. A. Jimenez, W. Saikaly, and A. Charai, *Mater. Charact.* **59**, 1607 (2008).
18. P. Nandi, S. Suwas, S. Kumar, and K. Chattopadhyay, *Metall. Mater. Trans. A* **44**, 2591 (2013).
19. A. Urrutia, S. Tumminello, D. G. Lamas, and S. Sommadossi, *Procedia Mater.Sci.* **8**, 1150 (2015).
20. Y. Castrillejo, A. Vega, M. Vega, P. Hernández, J. A. Rodriguez, and E. Barrado, *Electrochim. Acta* **118**, 58 (2014).
21. U. Kolemen, *J. Alloy. Compd.* **425**, 429 (2006).
22. O. Şahin, O. Uzun, S. L. Malgorzata, H. Göçmez, and U. Kolemen, *J. Eur. Ceram. Soc.* **28**, 1235 (2008).
23. M. F. Kılıçaslan, O. Uzun, F. Yilmaz, and S. Çaglar, *Metall. Mater. Trans. B* **45**, 1865 (2014).
24. O. Uzun, F. Yilmaz, U. Kolemen, and N. Basman, *J. Alloy. Compd.* **509**, 21 (2011).
25. S. Ruben, *Handbook of the Elements*, pp. 2,58,80, Open Court Pub. Co., Illionis, USA (1998).

26. U. Kolemen, O. Uzun, M. A. Aksan, N. Güçlü, and E. Yakinci, *J. Alloy. Compd.* **415**, 294 (2006).
27. S. J. Hong and C. Suryanarayana, *Metall. Mater. Trans. A* **36**, 715 (2005).
28. M. F. Kilicaslan, *J. Alloy. Compd.* **606**, 86 (2014).
29. W. G. Zhang, Y. C. Ye, L. J. He, P. J. Li, X. Feng, and L. S. Novikov, *Mat. Sci. Eng. A.* **578**, 35 (2013).
30. Y. L. Zhou and M. Niinomi, *Mater. T. JIM* **50**, 368 (2009).
31. J. Royset and N. Ryum, *Int. Mater. Rev.* **50**, 19 (2005).
32. J. Wang, Y. Du, S. L. Shang, Z. K. Liu, and Y. W. Li, *J. Min. Metall. Sect. B-Metall.* **50**, 37 (2014).
33. I. Alhayek and M. S. Gaith, *Jordan J. Mech. Indust. Eng.* **4**, 55 (2010).
34. F. Xu, Y. H. Ding, X. H. Deng, P. Zhnag, and Z. L. Long, *Physica B* **450**, 84 (2014).